Hindawi
Shock and Vibration
Volume 2021, Article ID 5561093, 9 pages
https://doi.org/10.1155/2021/5561093

*Research Article*

# Measurement and Analysis of Roadway Deformation and Stress under Mining-Induced Stress

**Jianfeng Cui**,[1,2] **Weijun Wang**,[1,2] **Qian Jia**,[1,2] **Gang Peng**,[1,2] **and Hai Wu**[1,2]

[1]*School of Resources, Environment and Safety Engineering, Hunan University of Science and Technology, Xiangtan, China*
[2]*Work Safety Key Lab on Prevention and Control of Gas and Roof Disasters for Southern Coal Mines, Hunan University of Science and Technology, Xiangtan, China*

Correspondence should be addressed to Weijun Wang; wjwang@hnust.edu.cn and Hai Wu; wuhai@hnust.edu.cn

Received 16 February 2021; Accepted 3 July 2021; Published 15 July 2021

Academic Editor: Pengfei Wang



Small coal pillars, which are used to protect roadways, have a significant influence on mining operations and roadway stability and safety. Consequently, the optimal width of coal pillars that provides suitable performance under mining-induced stress must be determined accurately. Based on the deformation data of the surrounding rock along the gob roadway of the 13318 working face in Xieqiao Coal Mine, we analyzed the surface deformation data of the roadway and the displacement of the deep surrounding rock of the roadway under the action of mining-induced stress herein. The separation fractures of the low side of the roadway can be divided into four zones: 0–2 m, 2–5 m, 5–9 m, and 9–11 m. The absolute displacement of the surrounding rock relative to the center of the roadway in the 0–2 m zone was large, and the displacement region in the side of the roadway extended from 0 m to 11 m. The separation fractures of the high side of the roadway can be divided into three zones: 0–3 m, 3–5 m, and 5–5.5 m. The absolute displacement of the surrounding rock relative to the center of the roadway in the 0–3 m zone was large, whereas the deformation separation of the coal pillar was small. The surrounding rock in the 5–5.5 m zone also exhibited absolute displacement relative to the center of the roadway. Furthermore, the stress increased faster on the low side of the roadway than the high side; the core stress region on the high side occurred at approximately 3 m, whereas that on the low side occurred at approximately 8 m. The findings obtained herein can help determine the optimal preset width of small pillars.

## 1. Introduction

Small pillars are often used in coal mining to protect roadways. The preset width of these small pillars directly affects the mining rate of the coal resources, roadway stability, and safety of the mining process. The width of the small pillars must be enough to ensure that they can withstand the effect of the front abutment pressure during roadway tunneling and advancing on the working face. Furthermore, the section area of the roadway should be able to meet the standards required for safe production even if the small pillars undergo deformation. Xu et al. [1] used theoretical and simulation methods to obtain the stress distribution, deformation characteristics, and plastic zone distribution around the roadway and coal pillars during roadway development and mining. Huang et al. [2] performed numerical simulations using FLAC3D to investigate the stability of coal pillars under different mining sequences. Xia et al. [3] used numerical methods to study the stability of mining roadways considering 6 m section coal pillars under the action of repeated mining.

Bao et al. [4] studied the large deformation mechanism of roadways in close and multicoal seam mining and revealed that the overlying coal pillar was the main influencing factor. Zheng et al. [5] analyzed the stress distribution of coal pillars of different widths during excavation and mining based on theoretical analyses, numerical simulations, and engineering practice. The results indicated that the width of the coal pillar should exceed 6 m as the deformation decreases with the increase in the width of the coal pillar. Han et al. [6] used numerical simulations to study the variation range of the plastic area of coal pillars of different

widths. The results revealed that the failure of a small coal pillar is significantly affected by its width. Furthermore, the outer edge of the pillar, that is, the area near the previous district sublevel goaf, was already in the plastic state.

Guo et al. [7] used an analytical theory and photoelastic experiment to study the laws of stress distribution and the displacement characteristics of the surrounding rock of a soft rock roadway. Wang et al. [8] numerically analyzed the characteristics of the stress and displacement of the surrounding rock damaged zone and plastic zone, considering the buried depth and lateral pressure coefficient. Liu et al. [9] analyzed the coal pillar vertical stress peak away from the coal wall. They observed that the roadway distance and the distance from the rear of the working face to the cutting seam depth have a logarithmic relationship. Jaiswal et al. [10] used various permutations and combinations of strain-softening parameters to establish a calibration model. They concluded that the pillars begin to yield at approximately two-thirds of the value of the peak strength. Furthermore, they developed statistical expressions to estimate the pillar strength in Indian coal mines and the postfailure modulus by analyzing the simulation results. Jia [11] studied the deformation laws of the roadway surrounding rock at different buried depths and compared the deformation laws of different roadways in the same coal mine. Wu et al. and Wang et al. [12, 13] analyzed the stability of a gob-side entry retaining roadway.

In this study, we perform field measurements of the displacement, surface deformation, and stress variation of the small pillars excavated along the goaf under the action of mining-induced stress. Subsequently, we perform an in-depth analysis to determine the influence of the mining-induced stress on the stability of small pillars and provide a basis to determine the preset width of a small pillar. In contrast to previous studies by Zhang et al. [14–17] and Wang et al. [18, 19], which primarily used numerical simulations and laboratory experimental research methods to determine the stress distribution and deformation characteristics of small coal pillars, the results obtained herein are based on actual on-site verification data.

## 2. Methods

*2.1. Stress Model of Roadway Surrounding Rock under the Action of Mining-Induced Stress.* Small pillars are widely used to protect roadways in coal mines in China. The width of these pillars is determined by the deformation characteristics and stress of the roadway surrounding rock and the small pillars. The coal and rock mass in the region where a small pillar is located are influenced by the roadway excavation of the previous working face, the mining of the previous working face, the roadway excavation of the current working face, and the advancing of the current working face. To simplify this analysis, a stress model of the surrounding rock along the goaf roadway was established as shown in Figure 1. Under the action of mining-induced stress, the small pillar deformations are composed of two parts: (1) the displacement of the small pillar surface toward the center of the roadway, which is caused by the separation expansion of the small pillar, and (2) the overall displacement of the small pillar toward the center of the roadway. The displacement of the solid coal side (low side), which moves toward the center of the roadway under the influence of the mining stress, is also composed of two parts: (1) the overall displacement of the solid coal side toward the roadway center and (2) the surface displacement toward the center of the roadway due to the separation and expansion of the solid coal side.

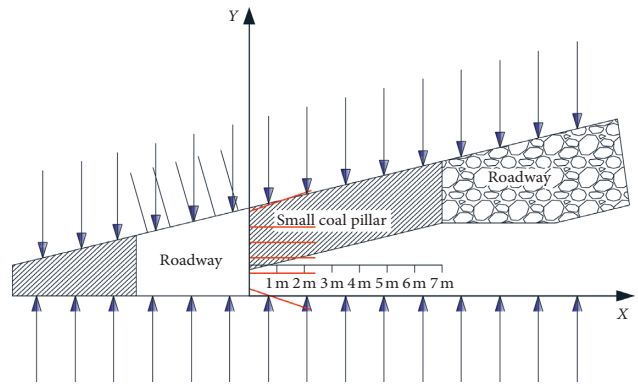


Figure 1: Schematic diagram of the stress model of the surrounding rock along the goaf.

*2.2. Conditions of Roadway Surrounding Rock and the Arrangement of the Monitoring Station under the Action of Mining-Induced Stress.* In the 13318 working face return air roadway of the Xieqiao Coal Mine, the width of the coal pillar is 7 m, the buried depth of the return air roadway in the working face is approximately −620 m, and the ground elevation is 20.8–27.6 m. The surrounding rock conditions in the test region are shown in Table 1.

The roadway support system is shown in Figure 2. The roof contains five high-strength rebar bolts (Ø20–Ø2200 mm), a 3.0 m long M4 steel band, a 10# diamond metal net (110 mm × 470 mm) combined support, with three Z2360 resin cartridges to lengthen bolting (the Z2360 resin cartridges have a diameter of 23 mm and a length of 60 mm, with a curing time of 91–180 s), a bolt row spacing of 1000 mm, and a bolt column spacing of 900 mm. The high side contains five high-strength rebar bolts (Ø20–Ø2200 mm), a 3.0 m long M4 steel band, and a 10# diamond metal net (110 mm × 470 mm) combined support. One of the root bolts (300 mm × 300 mm tray width) acts alone at a distance of 200 mm along the shoulder angle of the roadway roof, whereas the other four bolts are positioned according to the steel belt holes. Three Z2360 resin cartridges are used to lengthen bolting. The columnar distance between the bolts is 600 mm and the row distance is 900 mm. The low side contains four high-strength rebar bolts (Ø20–Ø2200 mm), a 3.0 m long M4 steel band, and a 10# diamond metal net (110 mm × 470 mm) combined support. One of the root bolts (300 mm × 300 mm tray width) acts alone at a distance of 200 mm along the shoulder angle of the roadway roof, whereas the other three bolts are positioned according to the steel belt holes. Three

Table 1: Comprehensive column diagram of the 13318 working face.

| Name of rock | Thickness (m) | Lithologic description |
|---|---|---|
| Medium fine quartz sandstone | 22.42 | Grayish white; medium to fine grain structure; fracture developed; predominately siliceous cementation; high quartz content; hard; locally contained pyrite veins |
| Sandy mudstone | 3.35 | Gray; arenaceous content is higher; only appears locally; the majority is absent |
| Mudstone | 0.55 | Gray; argillaceous structure; soft; mostly absent |
| No. 8 coal | 2.63 | Black; scaly; primarily bright coal; secondarily containing dark coal and silk carbon; visible pyrite film; appears as bright briquette |
| Mudstone | 1.44 | Gray to dark gray; upper clayey; homogeneous structure; horizontal bedding; fragile |
| Coal line | 0.34 | Grayish-black; blocky; mainly dark coal; local pinching out |
| Sandy mudstone | 2.57 | Dark gray; uneven fracture; pyrite veins and a few root fossils; uniform structure, with horizontal bedding; occasionally slow-wave bedding; fragile |
| 7–2 coal | 0.92 | Black; powdery; silk carbon; dark coal |
| Sandy mudstone | 6.46 | Gray to dark gray; primarily clayey upper part; lower part composed of silty sand and argillaceous material, which is composed of a thin layer, microhorizontal layer, and compact and occasionally carbonized bodies |

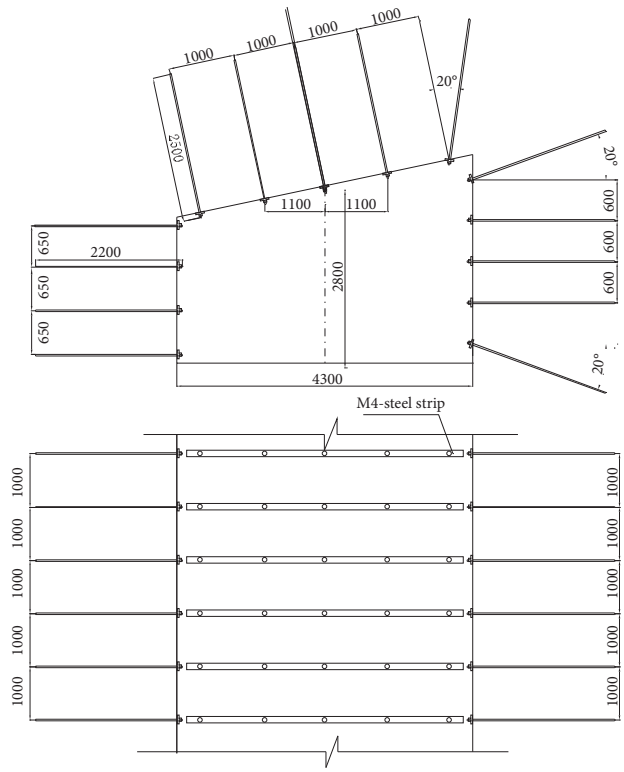


Figure 2: Bolt and cable support system of the roadway (units: mm).

Z2360 resin cartridges are used to lengthen bolting. The columnar distance between the bolts is 650 mm and the row distance is 900 mm.

The monitoring station is equipped with multiple-position borehole extensometers located at various intervals to measure the surface deformation and hydraulic borehole stress gauges. The layout of the monitoring station is shown in Figure 3. The surface deformation of the small pillar is measured at four different measuring points: B1, B2, B3, and B4. The cross section method is used to measure the total displacement of the high side, low side, roof, and floor. The multiple-position borehole extensometers were installed by drilling holes in the high and low sides of the roadway. In the roadway high side, these holes were drilled to depths of 1 m, 2 m, 3 m, 4 m, 5 m, and 5.5 m. In the roadway low side, these holes were drilled to depths of 1 m, 2 m, 3 m, 4 m, 5 m, 6 m, 9 m, and 11 m. Fourteen ZLGH-40 hydraulic borehole stress gauges were installed by drilling holes. Six were installed in the roadway high side at monitoring depths of 1 m, 2 m, 3 m, 4 m, 5 m, and 6 m, respectively, and eight were installed in the roadway low side at monitoring depths of 2 m, 4 m, 6 m, 8 m, 10 m, 12 m, 14 m, and 15 m, respectively.

The distance from the monitoring station to the working face was 80 m. The data were recorded immediately after installation, once a day. The recorded data includes the stress increase, surface deformation, and multiple-position extensometer data. The working face advances approximately 6–8 m per day.

## 3. Results and Discussion

*3.1. Deformation Test and Analysis of the Roadway.* Discrete mathematics is a mathematical discipline that studies the structure of discrete quantities and their mutual relationships and is an important branch of modern mathematics. Discrete mathematics implies that different elements are joined together. The object of the discrete quantities is usually a finite element or a countable element. Through interpolation and the average value method of discrete mathematics, the deformations recorded at the four measuring points were combined into one measuring point. Using Microsoft Excel, the displacement curves of the two sides and the roof-floor displacement curve were plotted based on the difference value of the structure. These are shown in Figures 4 and 5, respectively. The $x$-axis represents the distance advanced by the working face and the $y$-axis represents the displacement.

The displacement curves of the two sides (Figure 4) demonstrate that as the distance from the working face decreased, the total deformation of the high side, low side, and two sides of the roadway increased. The maximum deformation of the two sides was 854.4 mm, wherein the

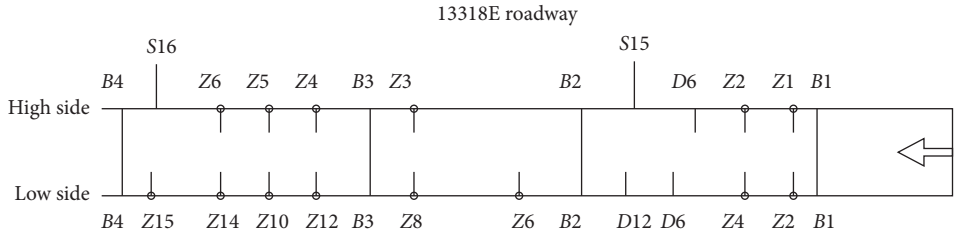


*Sx*: roadway length
*Bx*: *B* surface displacement, *x* the number
*Zx*: *Z* hydraulic borehole stress gauge, *x* the depth of monitor
*Dx*: multiple–position extensometer, *x* the depth of monitor

Figure 3: Layout of the monitoring station.

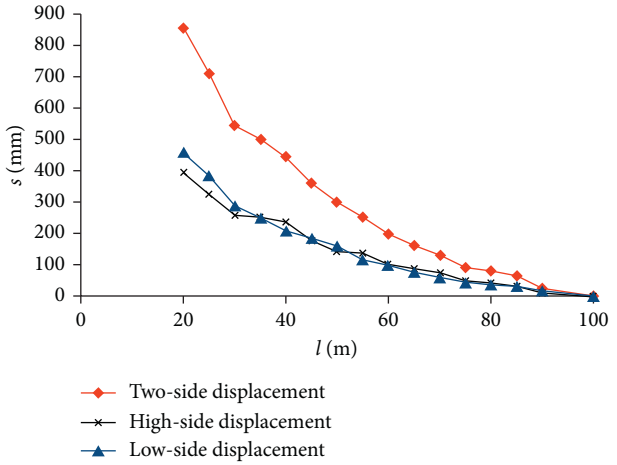


Figure 4: Regularity curve of displacement of the two sides after normalization.

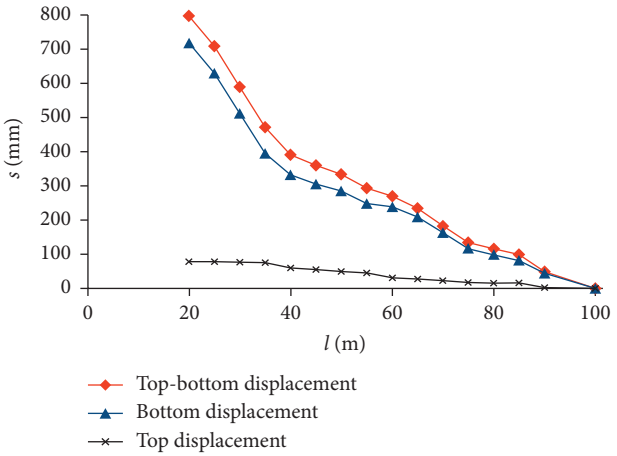


Figure 5: Regularity curve of displacement of the roof and floor after normalization.

deformation of the low side was 458.4 mm and that of the high side was 396 mm. Therefore, the low side deformation was 1.16 times that of the high side.

The displacement curves of the roof and floor (Figure 5) reveal that the displacement of the roof was 79.1 mm, that of the floor plate was 718.8 mm, and that of the roof and floor together was 797.9 mm. Therefore, the floor deformation was 9.08 times larger than that of the roof and accounted for 90% of the combined deformation of the roof and floor. The velocity of the roof deformation was the same 100–40 m away from the working face and increased from 40 m till the working face, although this increase was not large. When the distance advanced by the working face was less than 40 m, the increase in the floor deformation was small, and the deformation velocity increased sharply.

Using mathematical interpolation and average methods, the data obtained from two multiple-position borehole extensometers were combined, and the curves of the multipoint displacement of the low side and the high side were plotted using Microsoft Excel, as shown in Figures 6 and 7, respectively.

As shown in Figure 6, the values recorded at the measuring point at 1 m were the least, which indicates that the surrounding rock in the region of 0-1 m moves along with the low side surface toward the center of the roadway. The values at the measuring points at 2 m, 3 m, 4 m, 5 m, 6 m, 9 m, and 11 m were higher, which indicates that bed separation and capacity expansion occur at a depth of more than 1 m in the low side. However, the specific location of the separation development cannot be determined only from the values recorded by the multiple-position extensometers.

As shown in Figure 7, the values recorded at the measuring point at 1 m were the least, which indicates that the surrounding rock in the region of 0-1 m moves along with the high side surface toward the center of the roadway. The values recorded at the measuring points at 2 m, 3 m, 4 m, 5 m, and 5.5 m were higher, which indicates that bed-separation expansion occurs at a depth of more than 1 m from the surface of the small coal pillar. However, the specific location of the separation development cannot be determined only from the values recorded by the multiple-position extensometers.

Considering the surface displacement of the two sides of the roadway and the multiple-position extensometer values at each point (relative displacement), the displacement of each measuring point in each side relative to the center of the roadway (absolute displacement) $S_i$ can be calculated as

$$S_i = S_{\text{surface}} - S_{\text{read}}, \tag{1}$$

where $S_{\text{surface}}$ is the displacement from the roadway surface to the center of the roadway, $S_i$ is the absolute displacement

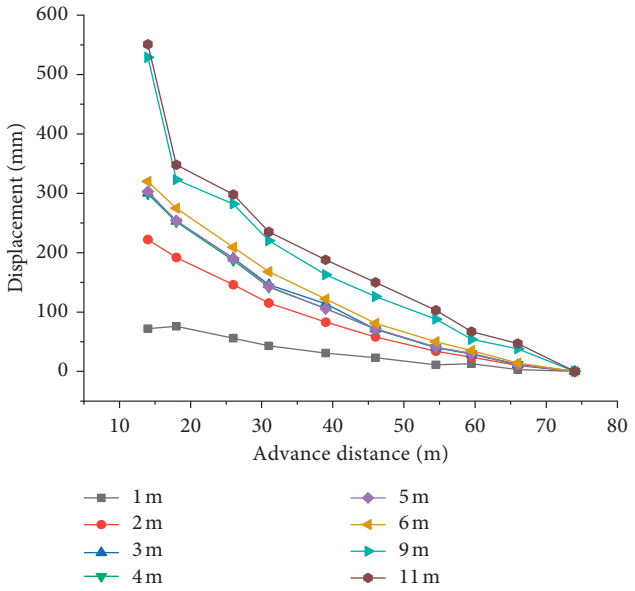


Figure 6: Displacement regularity curve of multiple points on the low side.

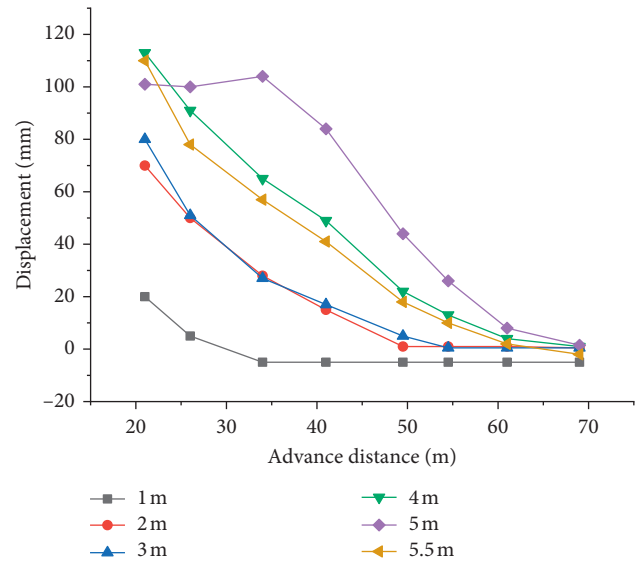


Figure 7: Displacement regularity curve of multiple points on the high side.

of each measuring point relative to the center of the roadway, and $S_{read}$ is the multiple-position extensometer reading at each measuring point.

Based on the calculated values of $S_i$, the absolute displacement curves of each measuring point in the high side and the low side, relative to the center of the roadway, were plotted using Microsoft Excel, as shown in Figures 8 and 9, respectively.

As shown in Figure 8, as the advance distance decreased, each measuring point of the multiple-position extensometer was further displaced toward the center of the roadway, but the extent of displacement differed. The low side of the roadway surface moved 458.5 mm toward the roadway center. The displacements of the measuring points at 1 m and 2 m toward the center of the roadway were 386 mm and 278.0 mm, respectively, which indicates that the 1-2 m zone experienced higher separation. The displacements of the measuring points at 3 m, 4 m, and 5 m toward the center of the roadway were 221.0 mm, 222.7 mm, and 220.5 mm, respectively, which indicates that the low side coal and rock mass in the 3–5 m zone moved toward the center of the roadway as a whole. The measuring point at 6 m moved 200.0 mm toward the center of the roadway, whereas the measuring point at 9 m moved 176.5 mm toward the center of the roadway. This indicates that the bed separation in the 6–9 m zone was relatively high. The measuring point at 11 m moved 160.5 mm toward the center of the roadway, which indicates that the bed separation in the 9–11 m zone was small. Each measuring point moved toward the center of the roadway as a whole, which indicates that the region of influence of the low side movement due to mining-induced stress exceeded 11 m.

As shown in Figure 9, as the advance distance decreased, each measuring point of the multiple-position extensometer was displaced toward the center of the roadway, but the

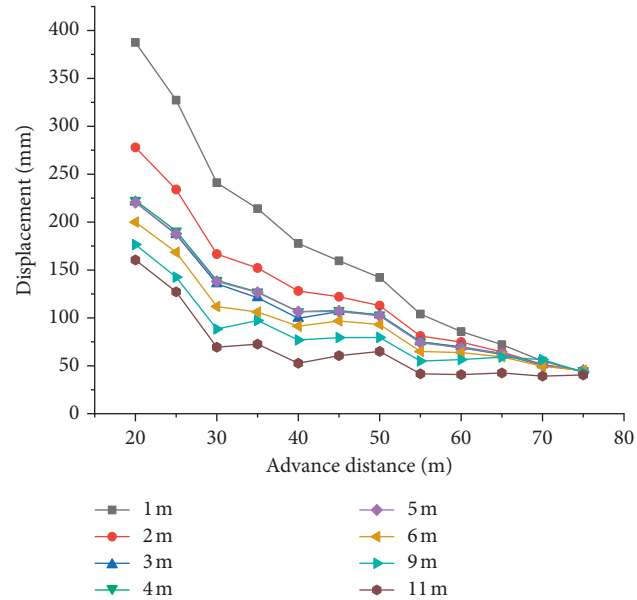


Figure 8: Absolute displacement of the measuring points on the low side.

extent of displacement differed. The high side of the roadway surface moved 396.0 mm toward the roadway center. The measuring point at 1 m moved 373.0 mm toward the center of the roadway; those at 2 m and 3 m moved 322.0 mm and 310 mm, respectively, toward the center of the roadway, which indicates that the 2-3 m zone moved toward the center of the roadway as a whole; and those at 4 m, 5 m, and 5.5 m moved 279.0 mm, 295.0 mm, and 280.0 mm, respectively, toward the center of the roadway, which indicates that the bed separation in the 4-5 m zone was large, whereas that in the 5-5.5 m zone was small. Furthermore, the data demonstrate that the region of influence of the coal pillar movement due to mining pressure exceeded 6 m.

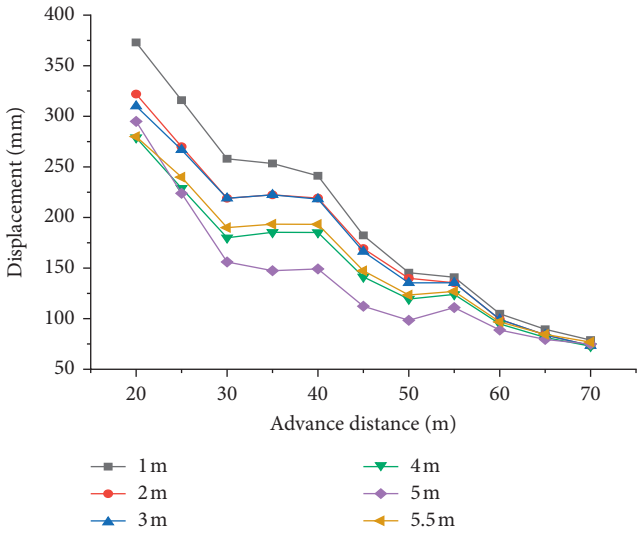


Figure 9: Absolute displacement of the measuring points on the high side.

*3.2. Test and Analysis of Stress of Roadway Surrounding Rock.* The variations in the stress of the measuring points at different depths in the roadway high and low sides with the advancing work face distance were obtained through continuous observation of the borehole deformation gauges. Microsoft Excel was used to plot the curve of the increase in stress at different depths in the roadway high and low sides with the variation in the advance distance, as shown in Figures 10 and 11, respectively.

As shown in Figure 10, on the roadway high side, the stress values in the drilled holes located 40–80 m behind the working face were small, with a maximum stress of approximately 2 MPa. As the distance to the working face reduced, the stress increased. The stress variation at a depth of 3 m was the highest, with a maximum value of 6.5 MPa. The stress variation between the depths of 3 m and 5 m was large, with a maximum variation of 4.13 MPa at 3 m and a minimum variation of 1.73 MPa at 1 m.

As shown in Figure 11, the stress in the drilled holes located 60–80 m away from the working face was small, with a maximum value of approximately 2.5 MPa. Beyond 60 m, the stress values increased with the decrease in distance from the working face. In particular, the stress variation at a depth of 8 m was the highest, with a maximum value of 18 MPa.

Based on the stress variation data at different depths in the roadway high and low sides, the vertical stress variation curves in the high and low sides at different advance distances were plotted using Microsoft Excel as shown in Figures 12 and 13, respectively.

As shown in Figure 12, the stress value at a depth of 4 m was the highest, whereas the stress values at depths of 1 m and 6 m were lower but distributed asymmetrically. The stress at a depth of 1 m was low, which indicates that the coal body in the shallow region of the high side was broken, considering its large deformation and relatively low stress. The borehole stress at 4 m was the highest, which indicates that the fracture degree of the central coal body in the 7 m coal pillar was low, and the stress was relatively high.

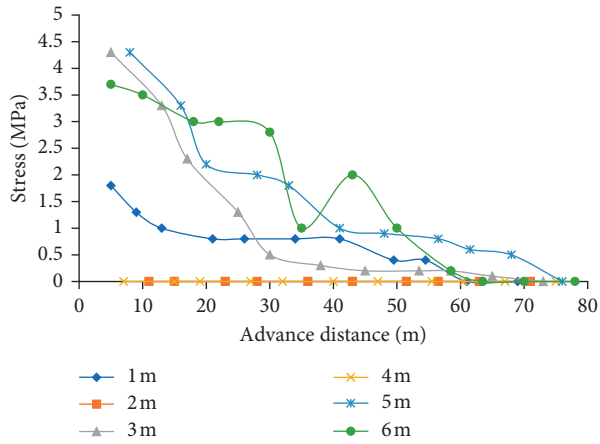


Figure 10: Stress curve at different depths on the high side.

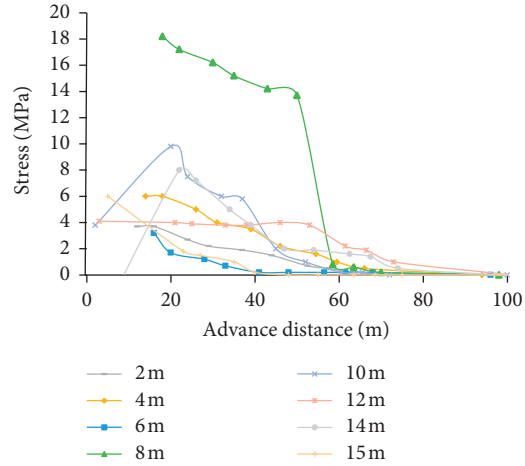


Figure 11: Stress curves at different depths on the low side.

As shown in Figure 13, the stress was maximum at a depth of 8 m, and the stress in the boreholes on both sides (shallow and deeper) was low. The stress values of the boreholes at depths of 4 m and 12 m formed two peaks. These indicate that the coal body in the low side shallow region was relatively broken and the stress values were relatively low. In particular, the stress in the 8 m deep borehole increased constantly and was maximum at a distance of 5 m from the working face.

Combined with the previous data, the three-dimensional distribution of the borehole stress in the high side and the low side was obtained as shown in Figures 14 and 15, respectively.

Combining Figures 10–15, the following conclusions can be drawn:

(1) The stress variations in the roadway high side due to mining-induced stress can be divided into three zones: infinite distance–80 m, 80–40 m, and 40–0 m. The stress variations in the roadway low side can also be divided into three zones: infinite distance–90 m, 90–60 m, and 60–0 m. The stress variation law of the high and low sides with the distance from the

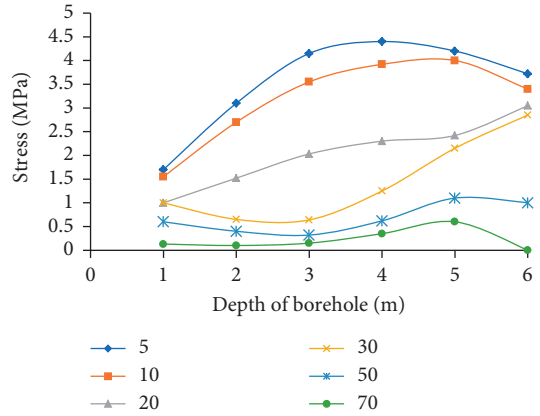


Figure 12: Stress variation in the high side at different advance distances.

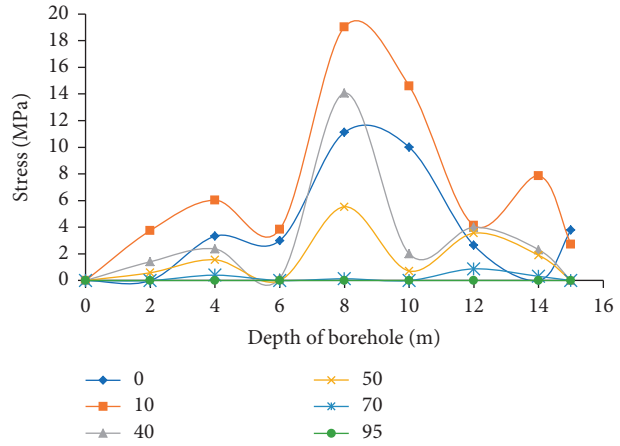


Figure 13: Stress variation in the low side at different advance distances.

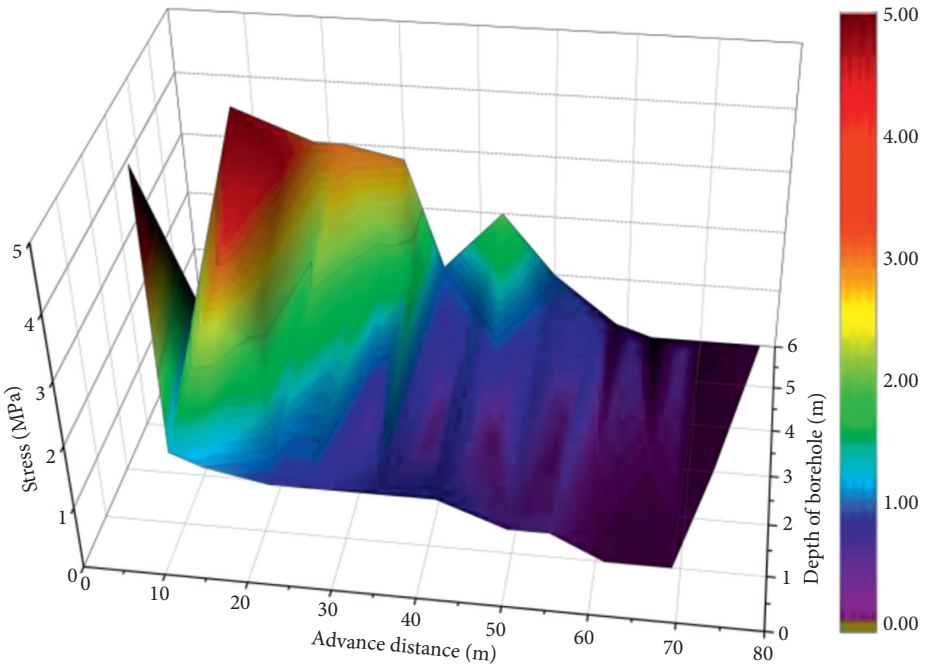


Figure 14: Three-dimensional variation in borehole stress in the high side.

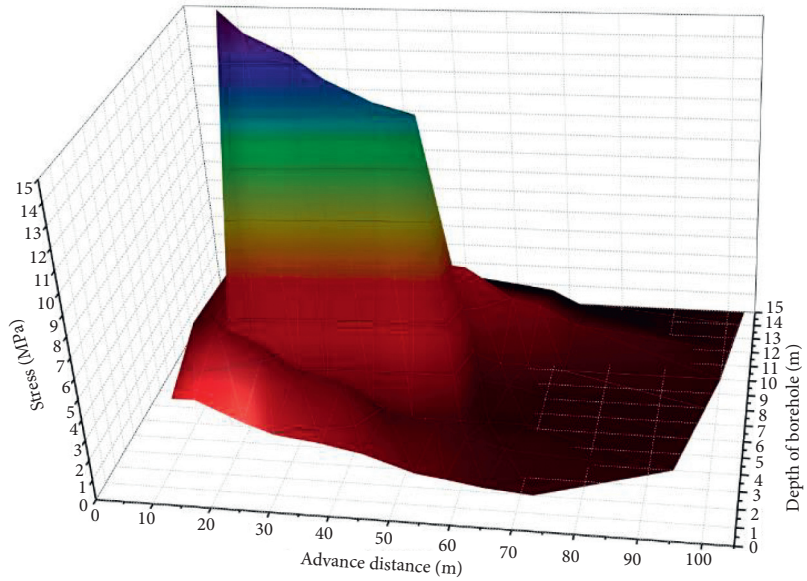


Figure 15: Three-dimensional variation in borehole stress in the low side.

working face of the mine is similar. However, the stress variation of the high side lags that of the low side. The increase in stress due to mining-induced stress on the low side is larger than that on the high side.

(2) The stress distribution indicates that a stress-bearing zone is formed on the high side, with a core region at approximately 3 m.

(3) The stress variation in the low side is complicated, with three peak values at different depths: 4 m, 8 m, and 12 m. The core region occurred at a depth of 8 m, and the maximum increase in stress occurred at this depth.

## 4. Conclusions

(1) Under the action of mining-induced stress, the bed-separation fractures in the low side of the roadway can be divided into four zones: 0–2 m, 2–5 m, 5–9 m, and 9–11 m. In the 0–2 m zone, the absolute displacement of the surrounding rock relative to the roadway center was large, and it was the main zone wherein separation fractures developed. In the 2–5 m zone, the absolute displacement of the surrounding rock relative to the roadway center was large, whereas the deformation and separation of the coal pillar were small. In the 5–9 m and 9–11 m zones, the absolute displacement of the surrounding rock relative to the roadway center was still observable, but the separation was less developed. Thus, the range of influence of the solid coal side displacement in the roadway extended beyond 11 m.

(2) Under the action of mining-induced stress, the bed-separation fractures in the high side of the roadway can be divided into three zones: 0–3 m, 3–5 m, and 5-5.5 m. In the 0–3 m zone, the absolute displacement of the surrounding rock relative to the roadway center was large, whereas the deformation and separation of the coal pillar were small. In the 3–5 m zone, the absolute displacement of the surrounding rock relative to the roadway center was large, and it was the main region wherein the separation of the coal pillar developed. In the 5-5.5 m zone, the absolute displacement of the surrounding rock relative to the roadway center was still observable, but the separation was less developed. Thus, the range of displacement of the small coal pillar extended beyond 5.5 m.

(3) Under the action of mining-induced stress, the stress in the high and low sides increased, but the rate of increase in stress was higher on the low side compared to the high side. The core stress region of the high side occurred at approximately 3 m, whereas that of the low side occurred at approximately 8 m.

## Data Availability

The data used to support the findings of this study are available upon request.

## Conflicts of Interest

The authors declare that they have no conflicts of interest.

## Acknowledgments

This work was supported by the National Natural Science Foundation of China (No. 51774133, No. 52074117) and the Hunan Provincial Natural Science Foundation (No. 2020JJ4305).

## References


[1] Q. Xu, J. Bai, S. Yan, R. Weng, and S. Wu, "Numerical study on soft coal pillar stability in an island longwall panel," *Advances in Civil Engineering*, vol. 2021, Article ID 8831778, 13 pages, 2021.

[2] J. Huang, F. Meng, G. Wang, Y. Wu, and J. Wan, "Simulation research for the influence of mining sequence on coal pillar stability under highwall mining method," *Geofluids*, vol. 2021, Article ID 8864339, 9 pages, 2021.

[3] Z. Xia, Q. Yao, G. Meng et al., "Numerical study of stability of mining roadways with 6.0-m section coal pillars under influence of repeated mining," *International Journal of Rock Mechanics and Mining Sciences*, vol. 138, Article ID 104641, 2021.

[4] Y. Bao, D. Su, and H. Mu, "Study on large deformation mechanism of roadway with close and multi coal seam in mining," *Geotechnical & Geological Engineering*, vol. 39, no. 3, pp. 1937–1949, 2021.

[5] X. Zheng, Z. Yao, and N. Zhang, "Stress distribution of coal pillar with gob-side entry driving in the process of excavation & mining," *Journal of Mining & Safety Engineering*, vol. 29, no. 4, pp. 459–465, 2012.

[6] C. Han, K. Zhang, X. Xu, D. Li, and P. Xie, "Study on failure regularity and reasonable dimension of district sublevel small coal pillar," *Journal of Mining & Safety Engineering*, vol. 24, no. 3, pp. 370–373, 2007.

[7] W. Guo, L. Li, and Y. Wang, "The photoelastic experiment simulating study on the law of stress distribution of the surrounding rock of soft rock roadway," *Journal of China Coal Society*, vol. 25, no. 6, pp. 596–600, 2002.

[8] H. Wang, D. Zhang, D. Deng et al., "Stress distribution characteristics of roadway surrounding rock damaged zone under non-hydrostatic pressure," *Journal of China Coal Society*, vol. 45, no. 11, pp. 3717–3725, 2020.

[9] Z. Liu, Y. Zhao, P. Gong et al., "Distribution characteristics of coal pillar stress after the roadway roof being large depth cutting seam," *Journal of China Coal Society*, vol. 36, no. 01, pp. 18–23, 2011.

[10] A. Jaiswal and B. K. Shrivastva, "Numerical simulation of coal pillar strength," *International Journal of Rock Mechanics and Mining Sciences*, vol. 46, no. 4, pp. 779–788, 2009.

[11] C. Jia, "Mechanism and control technology of surrounding rock instability in goaf roadway excavation of thick coal seam," *Journal of Mining and Rock Control Engineering*, vol. 2, no. 4, pp. 38–45, 2020.

[12] H. Wu, X. Wang, W. Yu, W. Wang, Z. Zhang, and G. Peng, "Analysis of influence law of burial depth on surrounding rock deformation of roadway," *Advances in Civil Engineering*, vol. 2020, Article ID 8870800, 13 pages, 2020.

[13] X. Wang, H. Wu, W. Wang, G. Peng, and Z. Zhang, "Deformation characteristics and mechanism of deep subsidize coal pillar of the tilted stratum," *Energy Science Engineering*, vol. 8, pp. 544–561, 2020.

[14] Z. Zhang, M. Deng, J. Bai, X. Yu, Q. Wu, and L. Jiang, "Strain energy evolution and conversion under triaxial unloading confining pressure tests due to gob-side entry retained," *International Journal of Rock Mechanics and Mining Sciences*, vol. 126, Article ID 104184, 2020.

[15] Z. Zhang, M. Deng, X. Wang, W. Yu, F. Zhang, and V. D. Dao, "Field and numerical investigations on the lower coal seam entry failure analysis under the remnant pillar," *Engineering Failure Analysis*, vol. 115, Article ID 104638, 2020.

[16] Z. Zhang, M. Deng, J. Bai, S. Yan, and X. Yu, "Stability control of gob-side entry retained under the gob with close distance coal seams," *International Journal of Mining Science and Technology*, vol. 31, 2020.

[17] Z. Zhang, J. Bai, Y. Chen, and S. Yan, "An innovative approach for gob-side entry retaining in highly gassy fully-mechanized longwall top-coal caving," *International Journal of Rock Mechanics and Mining Sciences*, vol. 80, pp. 1–11, 2015.

[18] H. Wang, Y. Jiang, Y. Zhao, J. Zhu, and S. Liu, "Numerical investigation of the dynamic mechanical state of a coal pillar during longwall mining panel extraction," *Rock Mechanics and Rock Engineering*, vol. 46, no. 5, pp. 1211–1221, 2013.

[19] H. Wang, B. A. Poulsen, B. Shen, S. Xue, and Y. Jiang, "The influence of roadway backfill on the coal pillar strength by numericalinvestigation," *International Journal of Rock Mechanics and Mining Sciences*, vol. 48, no. 3, pp. 443–450, 2011.